ECCOMAS Congress 2016
VII European Congress on Computational Methods in Applied Sciences and Engineering
M. Papadrakakis, V. Papadopoulos, G. Stefanou, V. Plevris (eds.)
Crete Island, Greece, 5–10 June 2016

ARTIFICIAL MICROSTRUCTURE GENERATOR FOR DUAL-PHASE STEELS

Y. Hou[1], A. Dumon[2], P. Culière[2] and M. Rachik[1]

[1]Laboratoire Roberval, CNRS UMR7337, Sorbonne universités, Université de technologie de Compiègne
Centre de recherche Royallieu, CS60319, 60203, Compiègne Cedex, France
e-mail: yuliang.hou@utc.fr, mohamed.rachik@utc.fr

[2] ESI Group
99 Rue des Solets, BP 80112, Rungis Cedex, France
e-mail: alexandre.dumon@esi-group.com, pierre.culiere@esi-group.com

Keywords: Dual-phase Steels, Microstructure Generator, Representative Volume Element, Homogenization, Proper Orthogonal Decomposition.

Abstract. *The microstructure of low alloyed ferritic-martensitic Dual-Phase (DP) steels consists of hard coarse grained martensite islands embedded in a soft ferrite matrix. Therefore, the macroscopic mechanical properties of DP steels mostly derive from their microstructures, such as volume fractions, morphology of martensite, phase distributions and ferrite grain size. Recently, micromechanical approaches are used to predict ductility and failure mode of DP steels under varying mechanical loading scenarios. In this work, an artificial microstructure generator inspired by topology optimization was developed to construct representative volume element (RVE) with predefined design parameters within a mofidied Voronoï tessellation. Micromechanical modeling of DP steel was performed on the generated artificial RVE. The plastic flow behavior of each single phase in DP steel were calculated by using a dislocation based theory. After numerical simulation, the flow curve on macro scale can be obtained from an asymptotic expansion homogenization (AEH) scheme. This approach allows studying the influence of individual microstructure features on local and global stress-strain response. To improve the robustness of this artificial microstructure generator, a proper orthogonal decomposition (POD) reduction was introduced to identify the optimal design parameters. This approach used a collection of artificial microstructures (snapshots) to find the most representative one of the real microstructure.*

1 INTRODUCTION

Advanced high strength steels (AHSSs), such as Dual-Phase (DP), Transformation Induced Plasticity (TRIP), Complex Phase (CP) and martensitic steels, have been developed and used in the automotive industry for the sake of reducing the weight of car body, improving passive safety performance, and fuel efficiency. DP steel usually consists of hard martensite islands embedded in a soft ferrite matrix, which makes it exhibit several mechanical characteristics, such as relatively high ultimate tensile strength (UTS), low yield to tensile strength ratio, absence of yield point elongation and a good balance of strength and formability [1, 2].

Recently, real microstructure based models of DP steel are created using experimental techniques, e.g., scanning electron microscopy (SEM), X-ray and neutron diffraction, and electron backscatter diffraction (EBSD), or statistical descriptions to study the influence of microstrutural featuers on the effective mechanical properties [3, 4, 5, 6]. However, highly inhomogeneous materials are formed during industrial welding, forging and heat treatment processes. Local microstructure varies significantly within the material, and is difficult to capture experimentally. It is comparatively easier to use a computed artificial microstructure based on local phase proportions and chemical compositions, which can be obtained from metal forming and heat-treatment simulations, e.g., SysWeld. This method particularly requires the development of an artificial microstructure with similar statistical properties to replace the real one.

Based on statistical descriptions of DP steel, artificial microstructures are commonly generated using geometry primitives (e.g., spheres, polygons or polyhedra). Al-Abbasi and Nemes [7] developed a micromechanical model for DP steel, which is dispersed of spherical martensitic particles with two different sizes in a ferritic matrix. However, this model has other disadvantages such as, inexact geometric representation and no reliable data close to the interface between different phases. Alternatively, Voronoï tessellation [8] is considered as an efficient tool for approximating the microstructure in DP steel.

In this study: firstly, a mofidied Voronoï tessellaion is periodically generated from Halton (quasi-random) sequence [9], which statistically exhibits low discrepancy, to provide adequate grain morphology. Secondly, two design parameters are proposed to control the phase assignment process in the DP steel. An algorithm related to density-based topology optimization method is introduced to solve the phase distribution problem. Thirdly, a proper orthogonal decomposition (POD) approach [10, 12] is applied to identify the optimal design parameters for a DP590 steel. Finally, micromechanial modeling are performed on the generated RVE using these optimal design parameters and the results corroborate experimental materials behavior.

2 MODIFIED VORONOI TESSELLATION

The concept of Voronoï tessellation allows to generate artificial polycrystalline aggregates with randomly distributed and oriented grains or cells for metallic or ceramic materials. This kind of aggregate is a nearest neighbor diagram determined from a set of generating points. Since the resulted diagram is mainly affected by the distribution of the Voronoï generating points, a modified point set has been applied to overcome the drawbacks (e.g., the inexact estimation of grain size and nearest neighboring grain number) found in the standard tessellation generated from a pseudo-random sequence [2]. Alternatively, the modified point set is generated using Halton (quasi-random) sequence, which statistically exhibits low-discrepancy [9].

Since periodic microstructures have favorable numerical properties in the context of computational homogenization, these seeds are repeated three times in each direction to ensure the periodicity of the modified Voronoï tessellation. In order to present the advantages of the mod-

ified Voronoï tessellation, an example has been compared with the standard one, as shown in Fig. 1 and 2. Two sets of seeds are generated using Halton (quasi-random) and pseudo-random sequences, as shown in Fig. 1a and b, respectively. The pairwise distance of each seed follows the same Gaussian distribution, as shown in Fig. 1c and d, in which the average value is 0.52 µm and the standard deviation is 0.25. These two parameters can be applied to control the average size of the generated Voronoï cells.

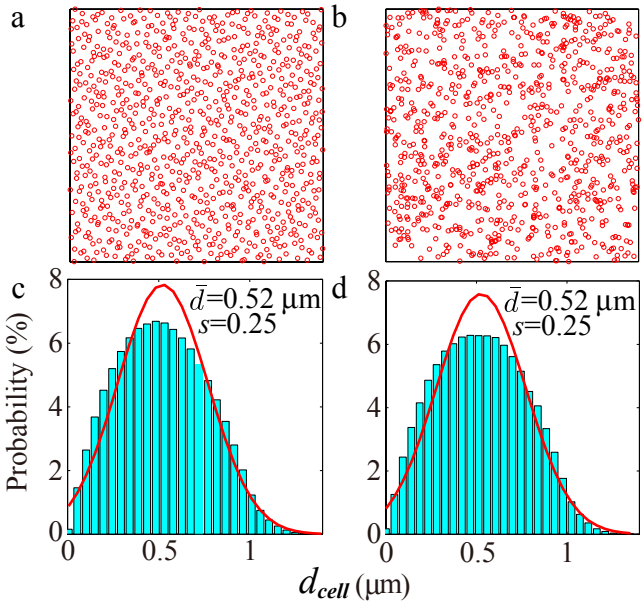

Figure 1: Scatter of periodic (a) modified and (b) standard Voronoï generating seeds including 900 points (30 points in each direction). Distribution of pairwise distance in each case: (c) modified and (d) standard generating seeds.

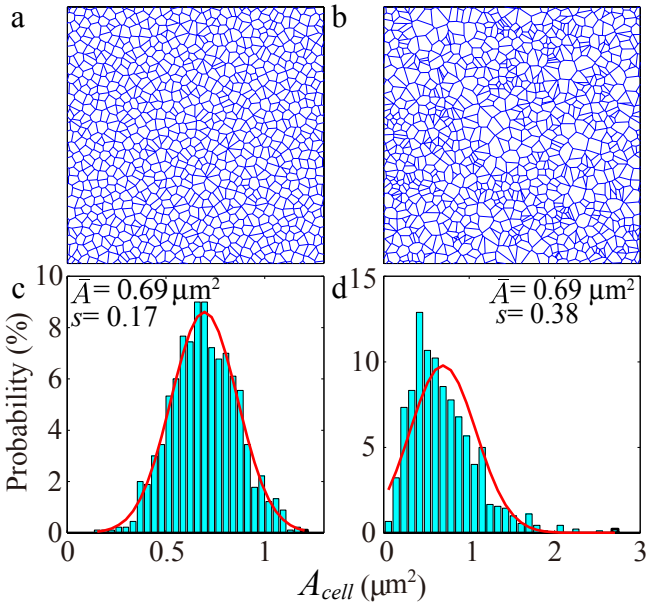

Figure 2: Square periodic Voronoï tessellations including 900 cells generated for: (a) modified one using Halton (quasi-random) sequence and (b) standard one using pseudo-random sequence. Distribution of cell area in each case: (c) modified and (d) standard tessellations.

Fig. 2a and b show the modified and standard Voronoï tessellations including 900 cells generated from the two seed sets. Fig. 2c and d also illustrate the area distribution of Voronoï cells for the modified and standard tessellations, respectively. From the comparison, both of the two generated Voronoï tessellations have the average cell area of $\bar{A}_{cell} = 0.69$ µm^2. However, the modified tessellation from Halton sequence shows a standard deviation of 0.17 which is less than half of the standard one (0.38). This clearly indicates that the modified Voronoï cells are more regular than the standard one. It can effectively avoid the appearance of bad aspect ratio and extremely small or large cells in the artificial polycrystalline aggregate, as shown in Fig. 3. This might cause that the variability of cell size is underestimated, while the number of nearest neighboring cells is overestimated.

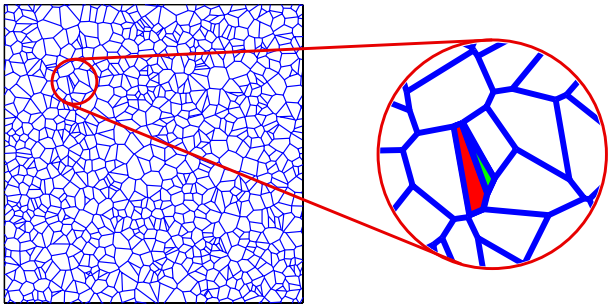

Figure 3: Voronoï cells with bad aspect ratio (red) and extremely small cell (green) in the standard Voronoï tessellation.

Usually, big martensite clusters are formed in the standard tessellation using the proposed phase assignment algorithm, which affect the formation of shear bands along the phase interface. It definitely leads to an inexact flow behavior prediction of DP steel. Moreover, the modified Voronoï tessellation is generated directly from Halton sequence, no additional computational cost on iteration to control the grain size distribution and grain morphology.

3 PHASE ASSIGNMENT ALGORITHM

With the modified Voronoï tessellation, an automate process need to be developed to assign the selected cells to represent different phases. Within this automate process, the modified Voronoï tessellation can be considered as a fixed grid, which is similar in material topology optimization design. In each modified Voronoï cell, a material density function is proposed to determine its phase property: martensite cells with density $\rho = 1$, the red layer in Fig. 4, while ferrite ones with density $\rho = 0$, the blue layer in Fig. 4. By defining constraints and an objective function, this process is deduced to a 0-1 decrete value optimization problem, also known as "black-and-white" design. Therefore, the material interpolation algorithms in topology optimization can be referred ti achieve artificial microstructures with proper phase distribution, as shown in Fig. 4.

In order to control the phase assignment, two design parameters proposed by Fillafer et al. [2], are utilized in this study to confine the solution space. These two parameters, the martensite phase fraction P_M and the neighboring coefficient of martensite grains C_M, which consider not only the martensite phase fraction but also the correlation of different martensite islands. The expressions of these two parameters are given as:

$$P_M = \frac{A_M}{A_T}, \quad C_M = \frac{2L_{MM}}{2L_{MM} + L_{FM}} \tag{1}$$

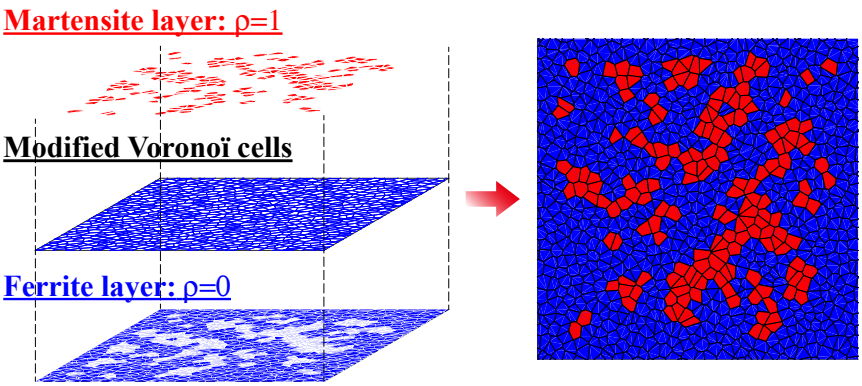

Figure 4: Automate phase assignment process and final DP microstructure.

where A_M and A_T denote martensite phase and total area, L_{MM} and L_{FM} are length of specific martensite-martensite and ferrite-martensite grain boundaries, respectively. Albeit it is identified that the value of P_M can vary between 0 and 1, for a given martensite phase fraction, C_M cannot satisfy the same range [2]. In other words, these two design parameters are not mutually independent.

According to the algorithm related to density-based topology optimization method, the design parameters can be rewritten in matrix form:

$$P_M = \frac{\mathbf{a}^T \boldsymbol{\rho}}{\mathbf{a}^T \mathbf{I}}, \quad C_M = \frac{\boldsymbol{\rho}^T \mathbf{E} \boldsymbol{\rho}}{\mathbf{I}^T \mathbf{E} \boldsymbol{\rho}} \tag{2}$$

where $\mathbf{a}$ is the grain area vocter, $\mathbf{E}$ is a correlation matrix of martensite islands' neighboring coefficient, $\mathbf{I}$ is uniform vector, and $\boldsymbol{\rho}$ is material density vector which only consists of 0 or 1:

$$\rho_e(\mathbf{x}) = \begin{cases} 0 & \text{if} \quad \mathbf{x} \in \Omega \backslash \Omega_M \\ 1 & \text{if} \quad \mathbf{x} \in \Omega_M \end{cases} \tag{3}$$

Noting from the definition of $\boldsymbol{\rho}$, a distributed and discrete value problem is formulated in the matrix form. To solve this problem, the most commonly used approach in topology optimization is to replace the integer by continuous variables. And then, a penality factor p is introduced to derive the martensite density distribution same as the so-called "black-and-white" solution [11, 13]. Therefore, a power form of the material density in each cell, also named "pseudo-density", can be rewritten as:

$$Q_e = Q_F + \rho_e^p (Q_M - Q_F) \tag{4}$$

where Q_F and Q_M are the material density of ferrite and martensite, respectively. Therefore, a structural optimization problem can be given as:

$$\begin{aligned} \textbf{Argmin} \quad & J = \| C_M - C_M^{target} \| \\ s.t.: \quad & \textstyle\int_\Omega Q_e(\mathbf{x}) \cdot \mathrm{a} \, d\Omega \leq P_M^{target} \cdot A_T \\ & Q_e \in [Q_F, Q_M] \end{aligned} \tag{5}$$

where the target design parameters P_M^{target} and C_M^{target} are predefined based on statistical descriptions of DP steel. Here, a heuristic updating scheme [11, 13] is introduced to solve this

optimization problem:

$$Q_e^{new}(\mathbf{x}) = \begin{cases} \max(0, Q_e - \delta) & \text{if} \quad Q_e B^\eta \leq \max(0, Q_e - \delta) \\ \min(0, Q_e + \delta) & \text{if} \quad Q_e B^\eta \geq \min(0, Q_e + \delta) \\ Q_e B & \text{otherwise} \end{cases} \tag{6}$$

where δ and η donate a positive move limit and a numerical damping coefficient, respectively. And, the term B is calculated using the optimality condition:

$$B = \frac{\dfrac{\partial J}{\partial Q_e}}{\lambda \dfrac{\partial P_M}{\partial Q_e}} \tag{7}$$

In Eq. (7), the Lagrangian multiplier λ is calculated using bisection algorithm to ensure the satisfaction of phase fraction constraint. Other two terms, $\partial J/\partial Q_e$ and $\partial P_M/\partial Q_e$ can be obtained in matrix form.

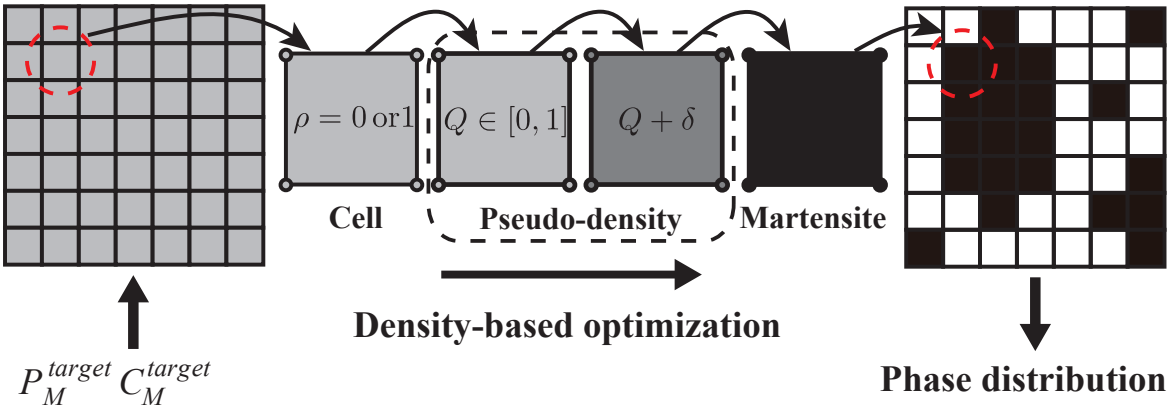

Figure 5: Illustration of the phase assignment algorithm inspired by topology optimization.

A schematic illustration of this phase assignment algorithm is shown in Fig. 5. In summary, the algorithm consists of the following step:

1. the initial material density of each Voronoï cell is given with the value of the target martensite phase fraction P_m^{target}, the initial grayscale grids in Fig. 5 (left);

2. the discrete material density is deduced to the continuous "pseudo-density", after the intergration of the penalization factor in Eq. (4). Meanwhile, this discrete value problem also becomes a continuous one;

3. iterations of the updating scheme in Eq. (6) is performed to achieve a convergent material density in each cell. The intermediate grayscale color in Fig. 5 (middle) shows the simultaneous material density after the first iteration;

4. a convergent solution is reached to present the optimal phase distribution. It is shown as the final grids in Fig. 5 (right), white and black fill colors indicate ferrite and martensite phases, respectively.

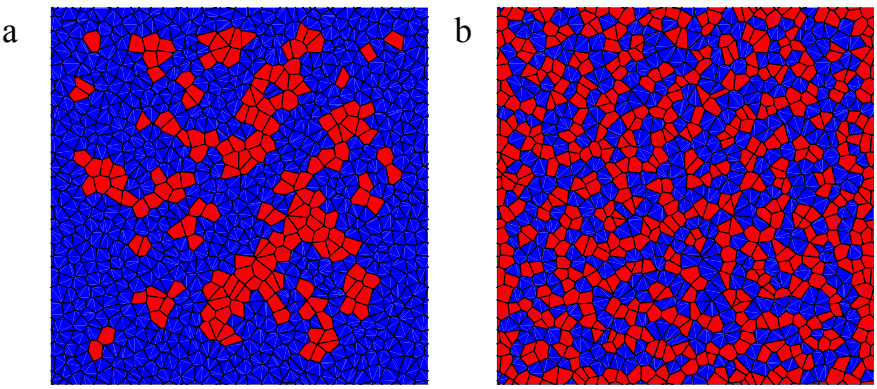

Figure 6: Example artificial microstructures with 900 grains: (a) $P_M = 0.22$, $C_M = 0.29$ ($P_M^{target} = 0.22$, $C_M^{target} = 0.3$) and (b) $P_M = 0.5$, $C_M = 0.5$ ($P_M^{target} = 0.5$, $C_M^{target} = 0.5$).

Following the aforementioned steps, artificial DP microstructures are constructed with a good convergence. That is, if the design parameters and the Voronoï tessellation are fixed, our generator will find only one unique optimal microstructure. Using the modified Voronoï tessellation described in Section 2 and predefined sets of design parameters, two example artificial microstructures are constructed as shown in Fig. 6.

In Fig. 6a, the target design paratmeters are set as $P_M^{target} = 0.22$ and $C_M^{target} = 0.3$. A fast and stable convergence is achieved in 9 iterations, the resulted microstructure is with $P_M = 0.22$ and $C_M = 0.29$. As discussed previously, due to the mutual independence of the two parameters, there exists a slight dissimilarity between the target and resulted parameters. While, an exact microstructure is constructed with target design parameters $P_M^{target} = 0.5$ and $C_M^{target} = 0.5$, as shown in Fig. 6b. It only takes 158 iterations to reach the convergence. This illustrates the flexibility of the proposed phase assignment algorithm in handling additional phase distribution parametric variables.

4 RESULTS AND DISCUSSION

In this study, the flow behavior of ferrite and martensite is obtained from a dislocation based theory [5], in which material parameters are calculated based on the local chemical composition. Numerical tensile test is performed on artificial RVEs generated with various design parameters. With the asymptotic expansion homogenization (AEH) method [14], each one can provide a prediction of flow behavior. In order to validate the proposed artificial microstructure generator, the generated RVE model is verified with a DP590 steel. The optimal design parameters $P_M = 0.22$ and $C_M = 0.3$ for the investigated DP590 steel are identified using a POD reduction approach, which considers the experimental measurement, as *a priori*. Therefore, the RVE generated by predefining the optimal design parameters within the modified Voronoï tessellation (Fig. 6a), is called as the optimal artificial RVE in the following content. Linear elements with 0.25 µm and plane strain assumption are applied in this study. Meshed FE models of the optimal artificial RVE of DP590 is shown in Fig. 7.

Tensile test simulation is performed on the optimal artificial RVE model by prescribing a periodic boundary condition. In the periodic boundary condition, a global plastic strain of 17% is imposed to deform the RVE models, which guarantees the material below the UTS. The resulted flow curves is compared with the experimental measurement, as shown in Fig. 8. A small discrepancy is observed between the simulated results and the measured curve. This can be attributed to the utilization of plane strain assumption, while the real specimen is subjected to 3D stress states. The similar difference has also been reported by Ramazani [6],

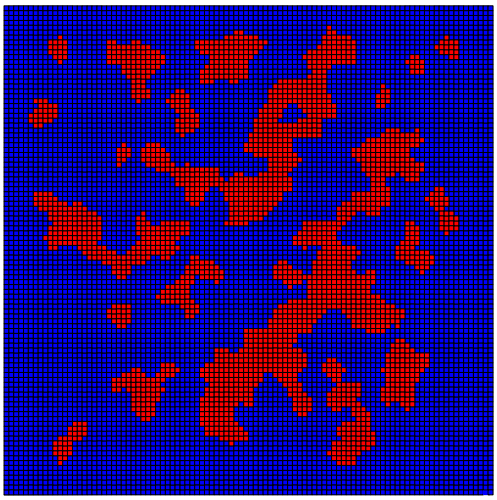

Figure 7: FE model with 0.25 µm element size and 25 µm edge length of the optimal artificial RVE for DP590 steel.

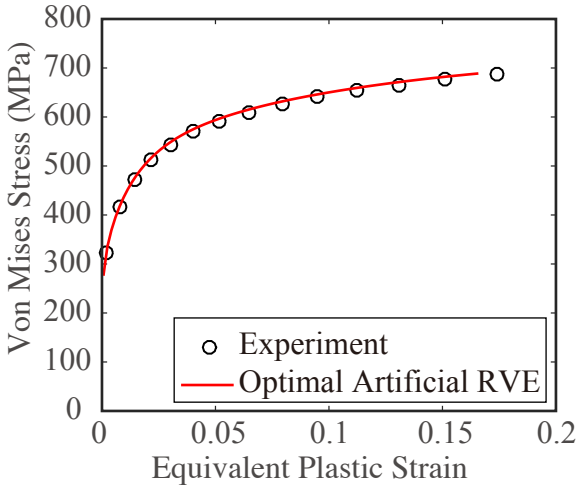

Figure 8: Comparison of flow curves between the experimental measurement and the predicted result of the optimal artificial RVE.

and it increases in the volume fraction of martensite. Nevertheless, the optimal artificial RVE provides an accurate prediction of flow behavior for the DP590 steel.

Fig. 9 show the equivalent plastic strain distribution in the optimal artificial RVEs at various global plastic strains. Although no material fracture or damage model is introduced, it is clearly found that shear bands are formed in the ferrite matrix near martensite grains (Fig. 9c). The shear bands and localized plastic strain are caused by the heterogeneous microstructure of DP590 steel. Further details are shown in Fig. 10, which indicates the equivalent plastic strain distribution at global strain of 15.8% in the optimal artificial RVE, and shear bands are located in the red ellipses. The direction of these shear bands is around 45° to the tensile loading. Integration of a ductile fracture model (e.g., GTN model) in the RVE model can be reasonably assumed to show nucleation of voids and microcracks in the strain localization zone, with the accumulation of plastic flow. Moreover, it is notable that, the validation of the optimal artificial microstructure is performed with the uniaxial tensile test. Due to the heterogeneity of the DP microstructure, additional investigations can be implemented in the case of biaxial or shear tests. This work will be performed in future studies.

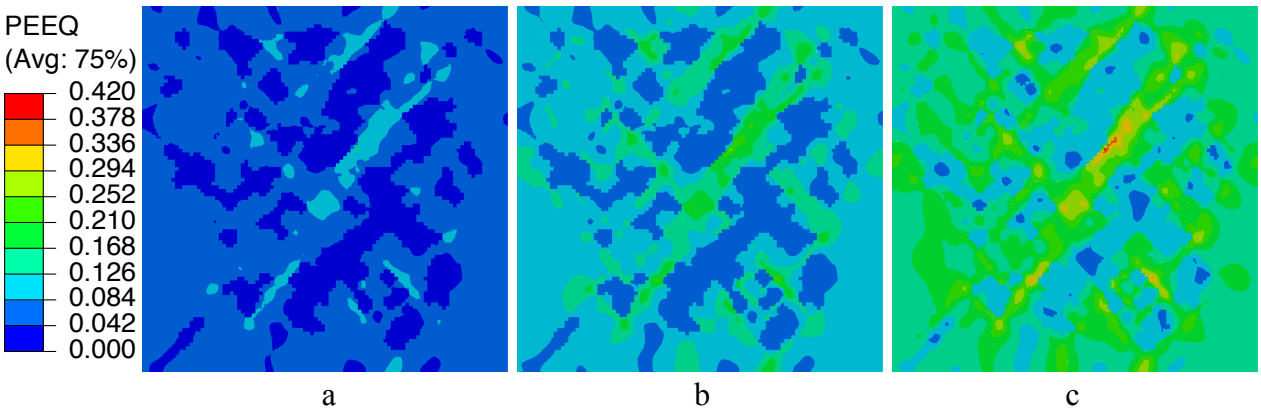

Figure 9: Equivalent plastic strain distribution in the optimal artificial RVE at global plastic strain levels of: (a) 5.09%, (b) 10.01% and (c) 15.03%

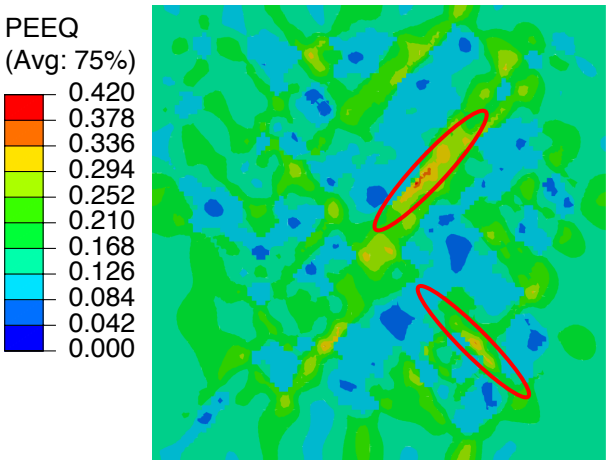

Figure 10: Equivalent plastic strain distribution at global plastic strain of 15.8% the optimal artificial RVE, shear bands in red ellipses.

5 CONCLUSION

In this study, we proposed a novel artificial generator inspired by topology optimization to reconstruct the microstructure of a DP steel. A modified Voronoï tessellation generated from Halton sequence, was utilized as the polycrystalline aggregate in the generator. Two microstructure parameters were introduced to control the phase assignment process in the DP steel. The novel phase assignment algorithm deduced the discrete value problem to a continuous one by defining a so-called "pseudo-density" within the modified Voronoï tessellation. Artificial DP microstructures were convergently generated with the optimal design parameters.

In order to validate the novel artificial generator, comparison of overall flow behavior was preformed between the experimental measurement and numerical simulation for a DP590 steel. It was shown that the optimal artificial RVE simulation can provide an accurate prediction. Moreover, shear bands were observed along the interface of different phase in each case. The path of shear bands is around 45° to the loading direction. It also concurs that, with the introduction of ductile fracture model, voids and microcracks can be formed in the strain localization zones. The promising results confirm the robustness of the proposed generator.

REFERENCES

[1] U. Liedl, S. Traint, E.A. Werner, An unexpected feature of the stress–strain diagram of dual-phase steel. *Computational Materials Science*. **25**, 180-192, 2002.

[2] A. Fillafer, C. Krempaszky, E.A. Werner, On strain partitioning and micro-damage behavior of dual-phase steels. *Materials Science and Engineering: A*. **614**, 122-128, 2014.

[3] X. Sun, K.S. Choi, A. Soulami, W. Liu, M.A. Khaleel, On key factors influencing ductile fractures of dual phase (DP) steels. *Materials Science and Engineering: A*. **526**, 140-149, 2012.

[4] H.T. Hossein, B. Anbarlooie, Javad. Kadkhodapour, G. Shadalooyi, Microstructural deformation pattern and mechanical behavior analyses of DP600 dual phase steel. *Materials Science and Engineering: A*. **600**, 108-121, 2014.

[5] A. Ramazani, K. Mukherjee, U. Prahl, W. Bleck, Modelling the effect of microstructural banding on the flow curve behaviour of dual-phase (DP) steels. *Computational Materials Science*. **52**, 46-54, 2012.

[6] A. Ramazani, K. Mukherjee, H. Quade, U. Prahl, W. Bleck, Correlation between 2D and 3D flow curve modelling of DP steels using a microstructure-based RVE approach. *Materials Science and Engineering: A*. **560**, 129-139, 2013.

[7] F.M. Al-Abbasi, J.A. Nemes, Micromechanical modeling of dual phase steels. *International Journal of Mechanical Sciences*. **45**, 1449-1465, 2003.

[8] G. Voronoï, Nouvelles applications des paramètres continus à la théorie des formes quadratiques. *Recherches sur les parallélloèdres primitifs, Deuxième mémoire*. **134**, 198-287, 1908.

[9] J.H. Halton, G.B. Smith, Radical inverse quasi-random point sequence, Algorithm 247. *Commun. ACM*. **7**, 701, 1964.

[10] L. Xia, B. Raghavan, P. Breitkopf, W. Zhang, Numerical material representation using proper orthogonal decomposition and diffuse approximation. *Applied Mathematics and Computation*. **224**, 450–462, 2013.

[11] L. Xia, P. Breitkopf, Design of materials using topology optimization and energy-based homogenization approach in Matlab. *Structural and multidisciplinary optimization*. **52**, 1229-1241, 2015.

[12] L. Meng, P. Breitkopf, B. Raghavan, G. Mauvoisin, O. Bartier, X. Hernot, Identification of material properties using indentation test and shape manifold learning approach. *Structural and multidisciplinary optimization*. **21**, 120-127, 2001.

[13] O. Sigmund, A 99 line topology optimization code written in Matlab. *Structural and multidisciplinary optimization*. **21**, 120-127, 2001.

[14] P.W. Chung, K.K. Tamma, R.R. Namburu, Asymptotic expansion homogenization for heterogeneous media: computational issues and applications. *Composites Part A: Applied Science and Manufacturing*. **32**, 1291-1301, 2001.